HHS Public Access

Author manuscript

Adv Mater. Author manuscript; available in PMC 2020 January 04.

Published in final edited form as:

Adv Mater. ; : e1803163. doi:10.1002/adma.201803163.

Dotted Core-Shell Nanoparticles for T_1-Weighted MRI of Tumors

Prof. Zheyu Shen,
CAS Key Laboratory of Magnetic Materials and Devices, & Key Laboratory of Additive Manufacturing Materials of Zhejiang Province, & Division of Functional Materials and Nanodevices, Ningbo Institute of Materials Technology and Engineering, Chinese Academy of Sciences, 1219 Zhong-guan West Road, Ning-bo, Zhe-jiang 315201, China.

Laboratory of Molecular Imaging and Nanomedicine, National Institute of Biomedical Imaging and Bioengineering, National Institutes of Health, Bethesda, Maryland 20892, United States.

Dr. Jibin Song,
Laboratory of Molecular Imaging and Nanomedicine, National Institute of Biomedical Imaging and Bioengineering, National Institutes of Health, Bethesda, Maryland 20892, United States.

Dr. Zijian Zhou,
Laboratory of Molecular Imaging and Nanomedicine, National Institute of Biomedical Imaging and Bioengineering, National Institutes of Health, Bethesda, Maryland 20892, United States.

Dr. Bryant.C. Yung,
Laboratory of Molecular Imaging and Nanomedicine, National Institute of Biomedical Imaging and Bioengineering, National Institutes of Health, Bethesda, Maryland 20892, United States.

Dr. Maria. A. Aronova,
Laboratory of Cellular Imaging and Macromolecular Biophysics, National Institute of Biomedical Imaging and Bioengineering, National Institutes of Health, Bethesda, Maryland 20892, United States.

Yan Li,
Key Laboratory of Applied Marine Biotechnology of Ministry of Education, Ningbo University, Ningbo 315211, China.

Dr. Yunlu Dai,
Laboratory of Molecular Imaging and Nanomedicine, National Institute of Biomedical Imaging and Bioengineering, National Institutes of Health, Bethesda, Maryland 20892, United States.

Dr. Wenpei Fan,
Laboratory of Molecular Imaging and Nanomedicine, National Institute of Biomedical Imaging and Bioengineering, National Institutes of Health, Bethesda, Maryland 20892, United States.

Dr. Yijing Liu*,

Correspondence to: Yijing Liu*; Xiaoyuan Chen*; Aiguo Wu*.
aiguo@nimte.ac.cn; shawn.chen@nih.gov; yijing.liu@nih.gov

Conflict of Interest
The authors declare no conflict of interest.

Supporting Information
Supporting Information is available from the Wiley Online Library or from the author

Laboratory of Molecular Imaging and Nanomedicine, National Institute of Biomedical Imaging and Bioengineering, National Institutes of Health, Bethesda, Maryland 20892, United States.

Zihou Li,
CAS Key Laboratory of Magnetic Materials and Devices, & Key Laboratory of Additive Manufacturing Materials of Zhejiang Province, & Division of Functional Materials and Nanodevices, Ningbo Institute of Materials Technology and Engineering, Chinese Academy of Sciences, 1219 Zhong-guan West Road, Ning-bo, Zhe-jiang 315201, China.

Huimin Ruan,
CAS Key Laboratory of Magnetic Materials and Devices, & Key Laboratory of Additive Manufacturing Materials of Zhejiang Province, & Division of Functional Materials and Nanodevices, Ningbo Institute of Materials Technology and Engineering, Chinese Academy of Sciences, 1219 Zhong-guan West Road, Ning-bo, Zhe-jiang 315201, China.

Dr. Richard. D. Leapman,
Laboratory of Cellular Imaging and Macromolecular Biophysics, National Institute of Biomedical Imaging and Bioengineering, National Institutes of Health, Bethesda, Maryland 20892, United States.

Dr. Lisen Lin,
Laboratory of Molecular Imaging and Nanomedicine, National Institute of Biomedical Imaging and Bioengineering, National Institutes of Health, Bethesda, Maryland 20892, United States.

Prof. Gang Niu,
Laboratory of Molecular Imaging and Nanomedicine, National Institute of Biomedical Imaging and Bioengineering, National Institutes of Health, Bethesda, Maryland 20892, United States.

Prof. Xiaoyuan Chen*, and
Laboratory of Molecular Imaging and Nanomedicine, National Institute of Biomedical Imaging and Bioengineering, National Institutes of Health, Bethesda, Maryland 20892, United States.

Prof. Aiguo Wu*
CAS Key Laboratory of Magnetic Materials and Devices, & Key Laboratory of Additive Manufacturing Materials of Zhejiang Province, & Division of Functional Materials and Nanodevices, Ningbo Institute of Materials Technology and Engineering, Chinese Academy of Sciences, 1219 Zhong-guan West Road, Ning-bo, Zhe-jiang 315201, China.

Abstract

Gd-based T_1-weighted contrast agents have dominated the magnetic resonance imaging (MRI) contrast agent market for decades. Nevertheless, they have been reported to be nephrotoxic and the U.S. FDA (food and drug administration) has issued a general warning concerning their use. In order to reduce the risk of nephrotoxicity, MRI performance of the Gd-based T_1-weighted contrast agents needs to be improved to allow a much lower dosage. In this study, novel dotted core-shell nanoparticles (FeGd-HN3-RGD2) with superhigh r_1 value (70.0 mM^{-1} s^{-1}) and very low r_2/r_1 ratio (1.98) were developed for high contrast T_1-weighted MRI of tumors. MTT assay and histological analyses showed good biocompatibility of FeGd-HN3-RGD2. LSCM images and flow cytometry demonstrated active targeting to integrin $\alpha_v\beta_3$ positive tumors. MRI of tumors showed high tumor ΔSNR for FeGd-HN3-RGD2 (477 ± 44 %), which is about 6–7-fold higher than that of

Magnevist (75 ± 11 %). MRI and ICP results further confirmed that the accumulation of FeGd-HN3-RGD2 in tumors was higher than liver and spleen due to the RGD2 targeting and small hydrodynamic particle size (8.5 nm), and FeGd-HN3-RGD2 was readily cleared from the body by renal excretion.

Keywords

magnetic resonance imaging; contrast agents; dotted core-shell nanoparticles; longitudinal relaxivity (r_1); transverse relaxivity (r_2)

Magnetic resonance imaging (MRI) is an attractive tool for clinical diagnosis utilizing an external magnetic field, radio waves, and a computer to generate specific images for the internal structures of a body.[1,2] Because it is noninvasive, does not require ionizing radiation that may cause harmful side effects, has a high spatial resolution, and has almost limitless tissue penetration depth, it has been widely used for the diagnosis of tumors,[3–5] Alzheimer's disease,[6] liver diseases,[7,8] bowel diseases,[9] and so on. In order to enhance the sensitivity of MRI, especially to clinically differentiate tumor from healthy tissues, MRI contrast agents are generally administered.[10,11] The MRI contrast agents include positive contrast agents generating bright signals that are also called T_1-weighted contrast agents,[12,13] and negative contrast agents generating dark signals that are also called T_2-weighted contrast agents.[14–16] The disadvantages of T_2-weighted contrast agents mainly include that the dark MRI images arising from T_2-weighted contrast agents are similar to that of hemorrhage, metal deposits, or calcification, and the T_2-weighted contrast agents can lead to a susceptibility artifact exhibiting unclear pictures due to their large magnetic moments. Therefore, the T_1-weighted contrast agents are universally accepted as better agents and have dominated the MRI contrast agent market for decades.[17,18] The reported exceedingly small magnetic iron oxide nanoparticles (ES-MIONs) are a kind of T_1-weighted MRI contrast agents due to the good biocompatibility. However, their longitudinal relaxivity (r_1) is relatively low (< 8.8 mM^{-1} s^{-1}, B_0 = 1.5 T). [18] The clinically used T_1-weighted contrast agents are Gd-based chelates that have been reported to be nephrotoxic, and the U.S. FDA (food and drug administration) has issued a general warning for their use, especially for patients with renal impairment.[19,20]

In order to reduce the risk of nephrotoxicity, the MRI performance of Gd-based T_1-weighted contrast agents need to be improved to allow a much lower dosage. Because the MRI performance is generally characterized by a signal-to-noise ratio (SNR), and the T_1-weighted contrast agents with high r_1 and low r_2/r_1 ratio (r_2 is transverse relaxivity) can induce high SNR,[18,21] enormous efforts in the past decade have been focused on the design and fabrication of various Gd-based T_1-weighted contrast agents with high r_1 value and low r_2/r_1 ratio. Zhou *et al.* developed Gd_2O_3-embedded iron oxide nanoplates (GdIOPs), whose r_1 value was 20.5 mM^{-1} s^{-1} and r_2/r_1 ratio was 7.1 (B_0 = 3.0 T).[22] Choi *et al.* designed a core-shell type nanoparticle with a core of $MnFe_2O_4$ (15 nm), a shell of $Gd_2O(CO_3)_2$ (1.5 nm), and a separating layer of SiO_2 (4, 8, 12, 16, 20 nm) (*i.e.* $MnFe_2O_4@SiO_2@Gd_2O(CO_3)_2$).[23] The maximum r_1 value was as high as 33.1 mM^{-1} s^{-1}, but the corresponding r_2/r_1 ratio was 8.3 (B_0 = 4.7 T), which is not low.[23] Li *et al.* reported

a synthesis of core-shell Fe_3O_4@Gd_2O_3 nanocubes, whose r_1 value was 45.24 mM^{-1} s^{-1} and r_2/r_1 ratio was 4.1 (B_0 = 1.5 T).[24] Yang *et al.* synthesized core-shell nanoparticles of Fe_3O_4@SiO_2 and covalently conjugated a Gd chelate (*i.e.* Gd-DTPA, DTPA is diethylenetriamine pentaacetic acid) and a RGD peptide (arginine-glycine-aspartic acid) on the surface. The r_1 value was 4.2 mM^{-1} s^{-1} and r_2/r_1 ratio was 4.1 (B_0 = 3.0 T).[25] Zhang *et al.* synthesized Gd doped iron oxide nanoparticles (GION) based on a thermal decomposition method, whose r_1 value was 7.87 mM^{-1} s^{-1} and r_2/r_1 ratio was 23.2 (B_0 = 9.4 T).[26] Jung *et al.* prepared Gd(III)-DOTA-modified sonosensitive liposomes using Gd(III)-DOTA-1,2-distearoyl-*sn*-glycero-3-phosphoethanolamine lipid. The r_1 value of the obtained Gd magnetoliposomes was 6.6 to 7.8 mM^{-1} s^{-1} (B_0 = 4.7 T), but the r_2/r_1 ratio was not provided.[27]

Overall, even considering the impact of B_0, the reported designs for Gd-based T_1-weighted contrast agents showed relatively high r_1 values, but their corresponding r_2/r_1 ratios were not sufficiently low. Herein, we report a kind of novel dotted core-shell nanoparticles with superhigh r_1 value of 73.5 mM^{-1} s^{-1} and very low r_2/r_1 ratio of 1.95 (B_0 = 1.5 T) for high contrast T_1-weighted MRI of tumors. Scheme 1 shows the design and synthesis of the hybrid nanoparticles. The seeds of exceedingly small magnetic iron oxide nanoparticles (ES-MIONs) were first synthesized by a coprecipitation method using poly(acrylic acid) (PAA) as a stabilizer. Gd^{3+} ions were then charged to be adsorbed onto the surfaces of ES-MION seeds *via* formation of ionic bonds between them and the –COOH groups from PAA. After that, gadolinium oxide nanoparticles (GdON) were synthesized *in situ* on the surface of ES-MION seeds to form three different structures at different feeding Gd concentrations (C_{Gd}). At medium feeding C_{Gd}, the obtained dotted core-shell type ES-MION/GdON hybrid nanoparticles (FeGd-HN) had a superhigh r_1 value and very low r_2/r_1 ratio. However, the obtained Gd-inserted type, or full core-shell type FeGd-HN at low or high C_{Gd} has a relatively low r_1 value and high r_2/r_1 ratio. Finally, a targeted ligand Glu-{Cyclo[Arg-Gly-Asp-(D-Phe)-Lys]}$_2$ (*i.e.* dimeric RGD peptide, or RGD2) was associated to the surface of the dotted core-shell type FeGd-HN to construct FeGd-HN-RGD2 nanoparticles for active targeting of tumors.

The synthesis conditions and characterization results of the FeGd-HN are summarized in Table S1. TEM images (Figure S1 a) show that FeGd-HN1–6 synthesized at various feeding Gd concentrations from 1000 to 62.5 mM have similar particle sizes (~ 5 nm), but FeGd-HN1 and 2 do not show as good dispersibility as FeGd-HN3–6. Due to the poor dispersibility, the hydrodynamic diameters (d_h) of FeGd-HN1 and 2 determined by DLS (Figure S1 b) are much larger than those of FeGd-HN3–6 (Table S1). The Fe recovery calculated from the molar ratio of Fe in the obtained nanoparticles to the feeding Fe is similar for FeGd-HN1–6 (83.2–89.3%) due to the same feeding Fe concentrations. However, the Gd recovery varies from 48.7% to 75.9% for FeGd-HN1–6 due to different feeding Gd concentrations. The Gd/Fe molar ratio in the resultant nanoparticles is calculated to be in the range of 0.81–0.07 for FeGd-HN1–6 (Table S1).

The r_1 and r_2 values of FeGd-HN1–6 are measured on a MRI scanner system (7.0 T, Bruker, B-C 70/16 US), and calculated according to the sum of Fe and Gd concentrations (*i.e.* C_{Fe+Gd}) (Figure S2 a, b, Table S1). Figure S2 c shows that the r_1 value increases and the

r_2/r_1 ratio decreases with increasing Gd/Fe molar ratio from 0.07 to 0.49, but the r_1 value decreases and r_2/r_1 ratio increases when the Gd/Fe molar ratio further increased from 0.49 to 0.81. The FeGd-HN3 had a higher r_1 value and lower r_2/r_1 ratio compared to FeGd-HN1 and FeGd-HN2 due to the higher Gd content. FeGd-HN4-FeGd-HN6 had lower r_1 values and higher r_2/r_1 ratios as compared to FeGd-HN3 due to the different structures (*i.e.* full core-shell type, and dotted core-shell type, Scheme 1).

$$\frac{1}{T_1} = \frac{q \quad P_m}{T_{1m} + \quad \tau_M} \quad (1)$$

In equation (1), $1/T_1$ is the longitudinal relaxation rate, q is the number of bound water molecules, and P_m is the mole fraction of water coordinated to the Gd center. The q and P_m values of full core-shell type FeGd-HN are smaller than that of dotted core-shell type FeGd-HN, which results in lower r_1 value and higher r_2/r_1 ratio. Therefore, FeGd-HN3 shows the best T_1-weighted MRI performance.

Figure S3 a shows the corresponding T_1-weighted MR images of FeGd-HN1–6 with various C_{Fe+Gd}, and Figure S3b shows ΔSNR of MR images in Figure S3 a. The signal-to-noise ratio (SNR) and ΔSNR (*i.e.* signal enhancement) were calculated according to the following equations:

$$\mathrm{SNR} = \frac{SI_{mean}}{SD_{noise}} \quad (2)$$

$$\Delta\mathrm{SNR} = \frac{SNR_{sample} - \quad SNR_{control}}{SNR_{control}} \times 100 \quad \% \quad (3)$$

The ΔSNR increases with increasing C_{Fe+Gd} for FeGd-HN1–6, and that of FeGd-HN3 is stronger than those of FeGd-HN1, 2, 4–6 at any C_{Fe+Gd}. This result further demonstrates that FeGd-HN3 is a better T_1-weighted contrast agent than FeGd-HN1, 2, 4–6.

The r_1 value of FeGd-HN3 measured at 7.0 T and calculated according to C_{Fe+Gd} is 6.92 ± 0.42 mM^{-1} s^{-1}, which is comparable to the reported GdIOPs (6.8 ± 1.3 mM^{-1} s^{-1}),[22] and much higher than that of ES-MIONs (2.40 mM^{-1} s^{-1})[18] and Magnevist® (3.54 mM^{-1} s^{-1}). In addition, the r_2/r_1 ratio of FeGd-HN3 (6.86 ± 0.31) is much lower than that of the GdIOPs (23.4),[22] but higher than that of Magnevist (1.47) (Table S1).

When calculated according to C_{Gd} instead of C_{Fe+Gd}, the r_1 value of FeGd-HN3 measured on 7.0 T was 21.0 ± 1.3 mM^{-1} s^{-1}, and the corresponding r_2 value and r_2/r_1 ratio were 143.9 ± 2.9 mM^{-1} s^{-1} and 6.86 ± 0.31, respectively (Figure S4 a, b, Table 1).

Figure S5 (Page S11) shows the plot of T_1 signal intensity *versus* TR. The T_1 signal intensity is saturated or almost saturated at any measured concentration. Figure S4 a, b (Page S10) show the fitting plots. The R^2 values of the fitting linear lines are all larger than 0.99. Figure S4 c (Page S10) shows the plot of T_1 *versus* T_2. The relationships are all linear. These results demonstrated the good quality of the obtained values.

In addition, the r_1 value of FeGd-HN3 measured on a clinical MRI scanner system (1.5 T, Magnetom Avanto, Siemens, Germany) is 73.5 ± 2.6 mM^{-1} s^{-1}, and the corresponding r_2 value and r_2/r_1 ratio are 143.0 ± 2.7 mM^{-1} s^{-1} and 1.95 ± 0.07, respectively (Figure S6, Table 1). The corresponding r_1 and r_2 values of the final FeGd-HN3-RGD2 were also measured on 1.5 T (Figure S7) and summarized in Table 1. The conjugation of RGD2 resulted in a lower r_1 value and higher r_2/r_1 ratio, which can be ascribed to the slight aggregation of the nanoparticles induced by RGD2 conjugation. Overall, as measured by a 1.5 T clinical MRI scanner system, the r_1 values of FeGd-HN3 and FeGd-HN3-RGD2 (>70.0 mM^{-1} s^{-1}) are much higher than the reported T_1-weighted MRI contrast agents[22–27] and Magnevist® (a commonly used T_1-weighted MRI contrast agent on the market). The corresponding r_2/r_1 ratios of FeGd-HN3 and FeGd-HN3-RGD2 (< 2.0) are lower than most of the reported T_1-weighted MRI contrast agents[22–27] and comparable to that of the Magnevist®. Therefore, FeGd-HN3 and FeGd-HN3-RGD2 with superhigh r_1 value and very low r_2/r_1 ratio are both promising T_1-weighted MRI contrast agents.

Figure 1 a, b shows the T_1-weighted MR images of FeGd-HN3-RGD2 and Magnevist® solutions at 200 μM of C_{Gd} with 250 or 100 ms of repetition time (TR) compared with pure water (control). From the black and white images and color images, we can see the MRI efficiency of our FeGd-HN3-RGD2 is much better than that of Magnevist®. Figure 1 c shows ΔSNR of the MR images for our FeGd-HN3-RGD2 and Magnevist® solutions in Figure 1 a, b compared to pure water. At 250 ms of TR, the ΔSNR is 819 ± 27 % for FeGd-HN3-RGD2 and 534 ± 35 % for Magnevist®. At 100 ms of TR, it is 1130 ± 29 % and 583 ± 72 %, respectively. The differences are statistically significant (*P < 0.001). These results reinforce the notion that FeGd-HN3-RGD2 nanoparticles are much better T_1-weighted MRI contrast agents than the commercially used Magnevist®.

The structure and elemental composition of our FeGd-HN1, 3, 6 were characterized *via* electron energy loss spectroscopic imaging (EELSI) in a scanning transmission electron microscopy (STEM) (Figure 2 a-c) and EELS spectra (Figure 2 d-f). To generate distributions of Fe, O and Gd, the background was subtracted and the signals for the Fe $L_{2,3}$ edge (710 eV), O K edge (530 eV), and Gd $M_{4,5}$ edge (1185 eV) were integrated over 10–20 eV wide energy windows above the core edges (Figure 2 a-c). From the overlay, it is evident that the concentration of Gd is decreasing on the surface of iron oxide cores, from for FeGd-HN1 (Figure 2 a), the hightest, FeGd-HN3 (Figure 2 b), to FeGd-HN6 (Figure 2 c), the lowest, which indicates full core-shell type, dotted core-shell type, and Gd-inserted type structures for FeGd-HN1, 3, and 6, respectively (Scheme 1). The EELS spectra (Figure 2 d-f) demonstrate that the elemental compositions of FeGd-HN1, 3, and 6 include O, Fe, and Gd, and the Gd content is high for full core-shell type FeGd-HN1, medium for dotted core-shell type FeGd-HN3, and low for Gd-inserted type FeGd-HN6, which are consistent with our synthesis design (Scheme 1).

The high resolution TEM (HR-TEM) images (Figure 3 a, b) show that the particle sizes of FeGd-HN3 and FeGd-HN3-RGD2 are similar at dry state. The size distributions measured by DLS (Figure 3 c) show that FeGd-HN3-RGD2 (d_h = 8.5 nm) is slightly larger than that of FeGd-HN3 (d_h = 6.5 nm) in aqueous solution. The energy dispersive X-ray spectra (EDS) (Figure 3 d) indicates that our FeGd-HN3 nanoparticles consist of Fe, Gd, and O elements. From field-dependent magnetization curves (Figure 3 e), the saturation magnetization (Ms) value is determined to be 11.5 and 12.4 emu/g for FeGd-HN3 and FeGd-HN3-RGD2, respectively. The slightly larger Ms value of FeGd-HN3-RGD2 can be ascribed to the slight aggregation of the nanoparticles induced by the conjugation of RGD2, which is consistent with the DLS results in Figure 3 c.

Figure S8 shows the zeta potential and stability study (shelf life) of FeGd-HN3-RGD2. The average zeta potential of FeGd-HN3-RGD2 (−14.8 mV), resulting from the –COOH group of PAA, provides electrostatic repulsion for colloidal stability. There is little to no change to the hydrodynamic diameter (d_h) of FeGd-HN3-RGD2 during storage for up to 30 days at 4 ^{o}C, which demonstrates good stability of FeGd-HN3-RGD2.

The cytotoxicity of FeGd-HN3-RGD2 *in vitro* was measured by MTT assay on U-87 MG cells (integrin $\alpha_v\beta_3$ positive)[28–30] and MCF-7 cells (integrin $\alpha_v\beta_3$ negative)[18], and compared with commercially available Magnevist® (Figure S9). Magnevist® shows low but detectable cytotoxicity on both U-87 MG and MCF-7 cells with ~ 90 % cell viability at 490 μM Gd, which is similar to the reported results.[31–33] FeGd-HN3-RGD2 shows much lower cytotoxicity on both U-87 MG and MCF-7 cells with > 97 % cell viability at 490 μM Gd. The lower cytotoxicity of FeGd-HN3-RGD2 can be ascribed from two points: 1) the Gd oxide is more biocompatible than Gd ion; 2) the Gd in FeGd-HN3-RGD2 nanoparticles is very hard to be released due to the stabilization by PAA because the Gd ion can be chelated with –COOH from PAA forming Gd-chelates. Therefore, the nephrotoxicity risk induced by FeGd-HN3-RGD2 is potentially lower than that of Magnevist® at the same Gd dosages.

To realize the active targeting of tumors, dimeric RGD peptide RGD2 was grafted to the surface of the FeGd-HN3 to construct FeGd-HN3-RGD2 nanoparticles. Figure S10 and S11 show the laser scanning confocal microscopy (LSCM) images of $\alpha_v\beta_3$ positive U-87 MG cells and $\alpha_v\beta_3$ negative MCF-7 cells incubated with Rhodamine 6G-loaded FeGd-HN3 (R6G-FeGd-HN3) or Rhodamine 6G-loaded FeGd-HN3-RGD2 (R6G-FeGd-HN3-RGD2). The cells untreated with nanoparticles are used as the control. The cytoskeleton stained with phalloidin-FITC is green and the nucleus is blue due to the Hoechst staining. The R6G-loaded nanoparticles are red. Figure 4 shows the corresponding merged LSCM images. It is obvious that lots of R6G-FeGd-HN3-RGD2 nanoparticles are uptaken by the U-87 MG cells, but very few are internalized for MCF-7 cells. In addition, very few R6G-FeGd-HN3 nanoparticles are internalized into both U-87 MG and MCF-7 cells. The above results indicate that the RGD2 conjugation can help $\alpha_v\beta_3$ positive cells uptake the nanoparticles, which indicates that our FeGd-HN3-RGD2 nanoparticles actively target $\alpha_v\beta_3$ positive tumors.

Figure S12 a-c shows the cellular uptake results of the nanoparticles measured by flow cytometry. The relative R6G fluorescence intensity of U-87 MG cells incubated with R6G-

FeGd-HN3-RGD2 is much higher than that of the U-87 MG cells incubated with R6G-FeGd-HN3, and MCF-7 cells incubated with R6G-FeGd-HN3 or R6G-FeGd-HN3-RGD2. Figure S12 d shows the corresponding quantitative results measured by ICP-OES (inductively coupled plasma optical emission spectrometry). The internalized Gd level by U-87 MG cells is determined to be 661 ± 59 fg/cell for R6G-FeGd-HN3-RGD2, and 113 ± 16 fg/cell for R6G-FeGd-HN3. The Gd level in the cells untreated with nanoparticles (control) is −5 ± 2 fg/cell. These results reinforce the hypothesis that our FeGd-HN3-RGD2 nanoparticles actively target $\alpha_v\beta_3$ positive tumors.

Our FeGd-HN3-RGD2 nanoparticles were also used as T_1 contrast agent for cancer cell MRI compared with Magnevist. Figure S13 a shows that the MRI signal of the U87 MG cells incubated with FeGd-HN3-RGD2 is much stronger than that of Magnevist. Figure S13 b shows ΔSNR of the MR images in Figure S13 a compared to the control, in which the cells were incubated with DMEM without contrast agent. The ΔSNR of FeGd-HN3-RGD2 is 121 ± 34 %, which is much stronger than Magnevist (54 ± 24 %) (* $P < 0.05$).

On the basis of MRI performance for both aqueous solutions and cancer cells, our FeGd-HN3-RGD2 and FeGd-HN3 were used for tumor detections on U-87 MG human glioblastoma bearing nude mice using commercially available Magnevist as a control. Figure 5 a-c shows the axial (slice orientation) T_1-weighted MR images of the tumor-bearing mice after intravenous injection of Magnevist, FeGd-HN3, or FeGd-HN3-RGD2 with 5.0 mg/kg of Gd dosage. It is obvious that the MRI signal is the strongest at 20 min, 4 h, or 6 h postinjection for Magnevist, FeGd-HN3, or FeGd-HN3-RGD2, respectively. The time point with strongest MRI signal depends on the size of contrast agent. It is 8.5 nm (d_h) for FeGd-HN3-RGD2 and 6.5 nm (d_h) for FeGd-HN3, which are both much larger than the small molecule Magnevist (Mw = 938.0). In addition, the MRI signal of FeGd-HN3-RGD2 at 6 h postinjection is much stronger than that of the FeGd-HN3 at 4 h postinjection due to the RGD2 active targeting to tumors, and they are both much stronger than that of Magnevist at 20 min postinjection due to their superhigh r_1 value and very low r_2/r_1 ratio (Table 1). Figure 5 d-f show the quantiative analysis of signal changes in tumors at different time points after contrast administration using ΔSNR. The SNR and ΔSNR were respectively calculated according to the equation (2) and (4).

$$\Delta\mathrm{SNR} = \frac{SNR_{post} - SNR_{pre}}{SNR_{pre}} \times 100\ \% \quad (4)$$

The highest tumor ΔSNR after intraveneous injection of our FeGd-HN3-RGD2 is 477±44 %, which is much higher than that of FeGd-HN3 (*i.e.* 342±47 %) and Magnevist (75±11 %). To the best of our knowledge, the 477 ± 44 % ΔSNR is arguably the highest as compared with the reported values, which are typically smaller than 210 %.[18,22,34,35]

We further investigated the MRI performance of FeGd-HN3-RGD2 nanoparticles and Magnevist at low dosage of 0.5 mg / kg (Figure S14). The tumor MRI signals after intravenous injection of FeGd-HN3-RGD2 nanoparticles are much stronger than those of

Magnevist (Figure S14 a, b). At low dosage of 0.5 mg/kg, the highest tumor ΔSNR after intraveneous injection of FeGd-HN3-RGD2 is 84 ± 9 %, which is much higher than that of Magnevist (12 ± 7 %) (Figure S14 c, d). More importantly, the highest tumor ΔSNR of FeGd-HN3-RGD2 at low dosage of 0.5 mg / kg (84 ± 9 %) is even higher than that of Magnevist at high dosage of 5.0 mg/kg (75 ± 11 %). These results demonstrate that FeGd-HN3-RGD2 is a better contrast agent than Magnevist, and the Gd dosage could be reduced by one order of magnitude thus potentially of lower nephrotoxicity risk.

We also compared the tumor accumulation of our FeGd-HN3-RGD2 to its liver uptake because, usually, the liver can readily take up nanoparticles through the macrophages of the reticuloendothelial system (RES).[36–38] Figure S15 a, b shows the coronal (slice orientation) T_1-weighted MR images of tumors and livers in U87 MG tumor-bearing nude mice after intravenous injection of our FeGd-HN3-RGD2 with 5.0 mg/kg of Gd dosage. It is obvious that the MRI signals of tumors and livers are enhanced over time, and reach a peak at 6 h postinjection, which is consistent with the above-mentioned results (Figure 5). Figure S15 c, d show the quantitative analysis of signal changes in the tumors and livers at different time points after contrast administration using ΔSNR. The highest tumor ΔSNR after intraveneous injection of our FeGd-HN3-RGD2 is 403 ± 37%, which is much larger than the highest liver ΔSNR (*i.e.* 266 ± 50%). However, high liver uptake of FeGd-HN3-RGD2 over Magnevist (small molecule) due to its larger size resulted in high SNR of liver (Figue S15), which leads to a relatively low contrast to noise ratio (CNR) of tumor to liver. The CNR and ΔCNR are calculated according to the equation (5) and (6).

$$\mathrm{CNR} = \frac{\left|SNR_{tumor} - SNR_{normal\ organ}\right|}{SNR_{tumor}} \quad (5)$$

$$\Delta\mathrm{CNR} = \frac{\left|CNR_{post} - CNR_{pre}\right|}{CNR_{pre}} \quad (6)$$

Although FeGd-HN3-RGD2 has a very high ΔSNR of tumor, the relatively low ΔCNR of tumor to liver is a disadvantage, which indicates that our FeGd-HN3-RGD2 is not a good contrast agent for MRI of lesions in the liver region. To overcome this disadvantage, further study is warranted to reduce the liver uptake *via* conjugation of polymers such as polyethylene glycol (PEG).

We further reconfirmed the high tumor accumulation of our FeGd-HN3-RGD2 *via in vivo* biodistribution measured by ICP. Figure S16 a shows the biodistribution of Gd level in the U87 MG tumor-bearing nude mice after intravenous injection of FeGd-HN3-RGD2 with 5.0 mg/kg of Gd dosage at 6 h post-injection or 6 d post-injection. The Gd level at 6 h time point is 6.4 ± 2.1, 3.8 ± 1.3, and 9.3 ± 3.3%ID/g for liver, spleen, and tumors, respectively. The high tumor accumulation of our FeGd-HN3-RGD2 can be ascribed to the targeting molecule RGD2, and the small hydrodynamic particle size (*i.e.* 8.5 nm). In addition, the Gd levels in

different organs and tissues of U-87 MG tumor-bearing nude mice at 6 days post-injection of FeGd-HN3-RGD2 or commercial Magnevist are all very small (< 0.9 % ID/g of tissue) and comparable to those without injection (Figure S16 b). Therefore, we can conclude that there is no significant remaining Gd on these organs after 6 days for our FeGd-HN3-RGD2, which indicates that our FeGd-HN3-RGD2 can be cleared from the body.

Figure S17 shows the T_1-weighted MR images of U-87 MG tumor-bearing nude mice after intravenous injection of FeGd-HN3-RGD2 with 5.0 mg/kg of Gd dosage for analysis of the bladder. The MRI signal of the bladder is much stronger at 2, 4, and 6 h postinjection than that before injection (control), which demostrates that FeGd-HN3-RGD2 (8.5 nm in diameter, d_h) could be cleared from the body by renal excretion.

Figure S18 shows the histological analyses of major organs from a normal healthy nude mouse, U-87 MG tumor-bearing nude mouse, and U-87 MG tumor-bearing nude mouse with intravenous injection of FeGd-HN3-RGD2 (5.0 mg/kg of Gd dosage, 3 days postinjection). Compared with the healthy nude mouse without U-87 MG xenografts and the tumor-bearing nude mouse without treatment, the tumor-bearing nude mouse with treatment of FeGd-HN3-RGD2 did not exhibit toxicity to the major organs and tumors. In addition, no toxicity was found to the major organs including heart, kidneys, liver, lung, and spleen (Figure S19), after injection of FeGd-HN3-RGD2. Therefore, FeGd-HN3-RGD2 is a potentially biocompatible and safe contrast agent for T_1-weighted MRI of tumors.

In summary, we developed novel FeGd-HN3-RGD2 nanoparticles with superhigh r_1 value and very low r_2/r_1 ratio for high contrast T_1-weighted MRI of tumors. The r_1 value of FeGd-HN3-RGD2 is 70.0 mM^{-1} s^{-1}, which is much higher than the commercial and reported T_1-weighted MRI contrast agents. The corresponding r_2/r_1 ratio is 1.98, which is lower than most of the reported T_1-weighted MRI contrast agents and comparable to the commercial Gd-chelates. MTT assay and histological analyses (H&E staining) show good biocompatibility for our FeGd-HN3-RGD2 nanoparticles. LSCM images and flow cytometry demonstrate active targeting to $\alpha_v\beta_3$ positive tumors. MRI of sample solutions and cancer cells indicates the stronger MRI efficiency than the commercial agent Magnevist. MRI of tumors shows a superhigh tumor ΔSNR (> 400 %), which is much higher than the reported values (< 210 %). MRI and ICP results further confirm that the accumulation of our FeGd-HN3-RGD2 in tumors is higher than in livers and spleens due to the RGD2 targeting and small hydrodynamic particle size (*i.e.* 8.5 nm), and our FeGd-HN3-RGD2 is easily cleared from the body in part by renal excretion.

Experimental Section

Chemicals:

Poly(acrylic acid) (PAA, Mw = 1800), iron (III) chloride ($FeCl_3$, ≥ 97%), gadolinium (III) nitrate hexahydrate ($Gd(NO_3)_3 \cdot 6H_2O$, 99.9%), *N*-(3-Dimethylaminopropyl)-*N'*-ethylcarbodiimide (EDC, ≥ 97%), N-hydroxysuccinimide (NHS, 98 %), Rhodamine 6G (R6G), phalloidin-FITC, and Hoechst 33258 were purchased from Sigma-aldrich (USA). Iron (II) sulfate heptahydrate ($FeSO_4 \cdot 7H_2O$) was purchased from Acros organics. Glu-

{Cyclo[Arg-Gly-Asp-(D-Phe)-Lys]}$_2$ (*i.e.* dimeric RGD peptide, or RGD2, 97.92%, Mw = 1318.51) was purchased from C S Bio Co. (CA, USA 94025).

Synthesis of ES-MION/GdON hybrid nanoparticles (FeGd-HN):

40 mL of PAA (Mw = 1800) solution (4.0 mg/mL) was first purged with nitrogen (≥ 50 min) to remove oxygen. The polymer solution was then heated to reflux (100 ^{o}C). After that, a 0.8 mL mixture of iron precursors (500 mM $FeCl_3$ plus 250 mM $FeSO_4$) was quickly injected into the heated polymer solution, followed by addition of 12 mL of ammonia solution (28 %). The reaction was kept at 100 ^{o}C for 30 min under magnetic stirring to obtain the seeds of extremely small magnetic iron oxide nanoparticles (ES-MIONs). After that, 0.8 mL of $Gd(NO_3)_3$ (62.5 ~ 1000 mM) and 6.0 mL of ammonia solution (28 %) were added into the reaction system. The reaction was continued for 90 min under magnetic stirring at 100 ^{o}C to obtain the FeGd-HN. The ES-MIONs were synthesized by a similar method without addition of Gd precursor.[18]

Finally, the solutions were cooled down to room temperature. The obtained FeGd-HN and ES-MIONs were purified by membrane dialysis (MWCO 6–8 kDa) against Milli-Q water for 5 days with a daily change of the water. The purified FeGd-HN and ES-MIONs were concentrated by centrifugal ultrafiltration (Millipore, MWCO 3 kDa). The Fe and Gd concentrations of the solutions were measured by inductively coupled plasma optical emission spectrometry (ICP-OES; Agilent 5100). The Fe or Gd recovery of the FeGd-HN was calculated from the molar ratio of Fe or Gd in the obtained FeGd-HN to the feeding Fe or Gd. In addition, 2.0 mL of the nanoparticle solutions were dried at 70 ^{o}C to calculate the mass concentration of the nanoparticles (with Fe_3O_4, Gd_2O_3 and PAA).

Characterization of FeGd-HN:

Distributions of Fe, Gd, and O in the FeGd-HN nanoparticles were mapped using electron energy loss spectroscopic imaging (EELSI) in a scanning transmission electron microscope (STEM).[39–41] The EELSI data were acquired with a Tecnai TF30 transmission electron microscope (FEI, Inc.) equipped with a Quantum imaging filter (Gatan Inc.), operating at an accelerating voltage of 300 kV. STEM images containing 2048 × 2048 pixels were acquired using a high-angle annular dark-field (HAADF) detector (Fischione Instruments, Inc.). For small selected regions within the HAADF images, EELSI data were acquired with approximately 35 pixels x 35 pixels x 2048 energy channels, spanning energy losses from 445 eV to 1470 eV, with 0.5 eV/channel. The pixel size was approximately 1 nm x 1 nm, and the pixel dwell time 0.1 s.

Synthesis of FeGd-HN3-RGD2:

The RGD2 were conjugated onto the surface of FeGd-HN3 via the reaction between –COOH and –NH_2 in the presence of EDC/NHS. Typically, 10 μL of EDC (55 μmol) and 50 μL 13 mg/mL of NHS (5.65 μmol) were added into 5.0 mL of FeGd-HN3 solution (C_{Fe} = 3.10 mM, C_{Gd} = 1.61 mM, ice cold) under magnetic stirring. After that, 100 μL of RGD2 (5.0 mg/mL, 3.8 mM) were added into the mixtures. After 16 h of reaction at room temperature under magnetic stirring, the obtained FeGd-HN3-RGD2 were washed 3 times using Milli-Q water by centrifugal ultrafiltration (Millipore, MWCO 3 kDa) to remove

unreacted EDC, NHS, RGD2, and side product EDU, and finally dissolved in 5.0 mL of Milli-Q water.

Synthesis of Rhodamine 6G-loaded FeGd-HN3-RGD2:

To investigate the internalization of FeGd-HN3 or FeGd-HN3-RGD2 in cells by flow cytometry and laser scanning confocal microscopy (LSCM), Rhodamine 6G (R6G) was loaded onto the surface of FeGd-HN3 or FeGd-HN3-RGD2. Typically, 4.0 mL of FeGd-HN3 (C_{Fe} = 3.10 mM, C_{Gd} = 1.61 mM), or FeGd-HN3-RGD2 (C_{Fe} = 3.10 mM, C_{Gd} = 1.61 mM) were mixed with 0.7 mL of Rhodamine 6G (10 μM) under magnetic stirring at room temperature. After 24 h, the obtained R6G-FeGd-HN3 or R6G-FeGd-HN3-RGD2 solution was washed using Milli-Q water by centrifugal ultrafiltration (Millipore, MWCO 3 kDa) to remove free R6G. The resultant R6G-FeGd-HN3 or R6G-FeGd-HN3-RGD2 was dispersed in 4.0 mL of Milli-Q water.

Cellular Uptake of the Nanoparticles Measured by ICP:

2.0 mL of U-87 MG cells in complete growth medium were seeded into each well of a 6-well culture plate with a cell density of 1.0×105 cells/mL and allowed to adhere at 37 oC for 24 h. The growth medium was then replaced with fresh media (2.0 mL, without FBS) without or with FeGd-HN3-RGD2, or FeGd-HN3 (CGd = 80 μM). After further 2.0 h incubation, the cells were washed twice with PBS, treated with trypsin for 3.0 min, and then centrifuged at 500 × g for 5 min to remove the extracellular nanoparticles. The obtained cells were used for Gd measurement by ICP.

Supplementary Material

Refer to Web version on PubMed Central for supplementary material.

Acknowledgements

This work is supported in part by the Youth Innovation Promotion Association of the Chinese Academy of Sciences (2016269) (Z. S.), National Natural Science Foundation of China (Grant Nos. 51761145021, U1501501, and U1432114), Public Welfare Technology Application Research Project of Zhejiang Province (2017C33129), the National Key Research & Development Program (2016YFC1400600), Intramural Research Program (IRP), National Institute of Biomedical Imaging and Bioengineering (NIBIB), National Institutes of Health (NIH) (Grant No. ZIA EB000073), Hundred Talents Program of Chinese Academy of Sciences (2010–735).

References

[1]. Cassidy MC, Chan HR, Ross BD, Bhattacharya PK, Marcus CM, Nat. Nanotechnol. 2013, 8, 363. [PubMed: 23644571]

[2]. Wang S, Lin J, Wang Z, Zhou Z, Bai R, Lu N, Liu Y, Fu X, Jacobson O, Fan W, Qu J, Chen S, Wang T, Huang P, Chen X, Adv. Mater. 2017, *29*, 1701013.

[3]. Shang W, Zeng C, Du Y, Hui H, Liang X, Chi C, Wang K, Wang Z, Tian J, Adv. Mater. 2017, 29, 1604381.

[4]. Mi P, Kokuryo D, Cabral H, Wu H, Terada Y, Saga T, Aoki I, Nishiyama N, Kataoka K, Nat. Nanotechnol. 2016, 11, 724. [PubMed: 27183055]

[5]. Li C, Nat. Mater. 2014, 13, 110. [PubMed: 24452345]

[6]. Viola KL, Sbarboro J, Sureka R, De M, Bicca MA, Wang J, Vasavada S, Satpathy S, Wu S, Joshi H, Velasco PT, MacRenaris K, Waters EA, Lu C, Phan J, Lacor P, Prasad P, Dravid VP, Klein WL, Nat. Nanotechnol. 2015, 10, 91. [PubMed: 25531084]

[7]. Perez-Balderas F, van Kasteren SI, Aljabali AAA, Wals K, Serres S, Jefferson A, Soto MS, Khrapitchev AA, Larkin JR, Bristow C, Lee SS, Bort G, Simone FD, Campbell SJ, Choudhury RP, Anthony DC, Sibson NR, Davis BG, Nat. Commun. 2017, 8, 14254. [PubMed: 28198362]

[8]. Zhou Z, Tian R, Wang Z, Yang Z, Liu Y, Liu G, Wang R, Gao J, Song J, Nie L, Chen X, Nat. Commun. 2017, 8, 15468. [PubMed: 28516947]

[9]. Lauenstein TC, Umutlu L, Kloeters C, Aschoff AJ, Ladd ME, Kinner S, Acad. Radiol. 2012, 19, 1424. [PubMed: 22841341]

[10]. Gao Z, Hou Y, Zeng J, Chen L, Liu C, Yang W, Gao M, Adv. Mater. 2017, 29, 1701095.

[11]. Lee JH, Huh YM, Jun YW, Seo JW, Jang JT, Song HT, Kim S, Cho EJ, Yoon HG, Suh JS, Cheon J, Nat. Med. 2007, 13, 95. [PubMed: 17187073]

[12]. Shen Z, Wu A, Chen X, Mol. Pharmaceutics 2017, 14, 1352.

[13]. Ma XH, Gong A, Xiang LC, Chen TX, Gao YX, Liang XJ, Shen ZY, Wu AG, J. Mater. Chem. B 2013, 1, 3419.

[14]. Gao Z, Ma T, Zhao E, Docter D, Yang W, Stauber RH, Gao M, Small 2016, 12, 556. [PubMed: 26680328]

[15]. Shen Z, Wu H, Yang S, Ma X, Li Z, Tan M, Wu A, Biomaterials 2015, 70, 1. [PubMed: 26295434]

[16]. Ma X, Gong A, Chen B, Zheng J, Chen T, Shen Z, Wu A, Colloid. Surface. B 2015, 126, 44.

[17]. Wang H, Revia R, Wang K, Kant RJ, Mu Q, Gai Z, Hong K, Zhang M, Adv. Mater. 2017, 29, 1605416.

[18]. Shen Z, Chen T, Ma X, Ren W, Zhou Z, Zhu G, Zhang A, Liu Y, Song J, Li Z, Ruan H, Fan W, Lin L, Munasinghe J, Chen X, Wu A, ACS Nano 2017, 11, 10992. [PubMed: 29039917]

[19]. Thomsen HS, Eur Radiol. 2004, 14, 1654. [PubMed: 15221265]

[20]. Akgun H, Gonlusen G, Cartwright JR, Suki WN, Truong LD, Arch. Pathol. La*b. Med.* 2006, 130, 1354. [PubMed: 16948524]

[21]. Slobozhanyuk AP, Poddubny AN, Raaijmakers AJE, van den Berg CAT, Kozachenko AV, Dubrovina IA, Melchakova IV, Kivshar YS, Belov PA, Adv. Mater. 2016, 28, 1832. [PubMed: 26754827]

[22]. Zhou Z, Wu C, Liu H, Zhu X, Zhao Z, Wang L, Xu Y, Ai H, Gao J, ACS Nano 2015, 9, 3012. [PubMed: 25670480]

[23]. Choi JS, Lee JH, Shin TH, Song HT, Kim EY, Cheon J, J. Am. Chem. Soc. 2010, 132, 11015. [PubMed: 20698661]

[24]. Li F, Zhi D, Luo Y, Zhang J, Nan X, Zhang Y, Zhou W, Qiu B, Wen L, Liang G, Nanoscale 2016, 8, 12826. [PubMed: 27297334]

[25]. Yang H, Zhuang Y, Sun Y, Dai A, Shi X, Wu D, Li F, Hu H, Yang S, Biomaterials 2011, 32, 4584. [PubMed: 21458063]

[26]. Zhang G, Du R, Zhang L, Cai D, Sun X, Zhou Y, Zhou J, Qian J, Zhong K, Zheng K, Kaigler D, Liu W, Zhang X, Zou D, Wu Z, Adv. Funct. Mater. 2015, 25, 6101.

[27]. Jung SH, Na K, Lee SA, Cho SH, Seong H, Shin BC. Nanoscale Res. Lett. 2012, 7, 462. [PubMed: 22901317]

[28]. Park SH, Zheng JH, Nguyen VH, Jiang SN, Kim DY, Szardenings M, Min JH, Hong Y, Choy HE, Min JJ, Theranostics 2016, 6, 1672. [PubMed: 27446500]

[29]. Chen H, Niu G, Wu H, Chen X, Theranostics 2016, 6, 78. [PubMed: 26722375]

[30]. Melemenidis S, Jefferson A, Ruparelia N, Akhtar AM, Xie J, Allen D, Hamilton A, Larkin JR, Perez-Balderas F, Smart SC, Muschel RJ, Chen X, Sibson NR, Choudhury RP, Theranostics 2015, 5, 515. [PubMed: 25767618]

[31]. Hung AH, Holbrook RJ, Rotz MW, Glasscock CJ, Mansukhani ND, MacRenaris KW, Manus LM, Duch MC, Dam KT, Hersam MC, Meade TJ, ACS Nano 2014, 8, 10168. [PubMed: 25226566]

[32]. Mi P, Kokuryo D, Cabral H, Kumagai M, Nomoto T, Aoki I, Terada Y, Kishimura A, Nishiyama N, Kataoka K, J. Control. Release 2014, 174, 63. [PubMed: 24211705]

[33]. Hou Y, Qiao R, Fang F, Wang X, Dong C, Liu K, Liu C, Liu Z, Lei H, Wang F, Gao M, ACS Nano 2013, 7, 330. [PubMed: 23199030]

[34]. Zhang H, Li L, Liu XL, Jiao J, Ng CT, Yi JB, Luo YE, Bay BH, Zhao LY, Peng ML, Gu N, Fan HM, ACS Nano 2017, 11, 3614. [PubMed: 28371584]

[35]. Zhou Z, Wang L, Chi X, Bao J, Yang L, Zhao W, Chen Z, Wang X, Chen X, Gao J, ACS Nano 2013, 7, 3287. [PubMed: 23473444]

[36]. Liu Z, Cai W, He L, Nakayama N, Chen K, Sun X, Chen X, Dai H, Nat. Nanotechnol. 2007, 2, 47. [PubMed: 18654207]

[37]. Maldiney T, Bessiere A, Seguin J, Teston E, Sharma SK, Viana B, Bos AJJ, Dorenbos P, Bessodes M, Gourier D, Scherman D, Richard C, Nat. Mater. 2014, 13, 418. [PubMed: 24651431]

[38]. Du B, Jiang X, Das A, Zhou Q, Yu M, Jin R, Zheng J, Nat. Nanotechnol. 2017, 12, 1096. [PubMed: 28892099]

[39]. Aronova MA, Leapman RD, Mat. Res. Soc. Bulletin 2012, 37, 53.

[40]. Myroshnychenko V, Nelayah J, Adamo G, Geuquet N, Rodriguez-Fernandez J, Pastoriza-Santos I, MacDonald KF, Henrard L, Liz-Marzan LM, Zheludev NI, Kociak M, Garcia de Abajo FJ, Nano Lett. 2012, 12, 4172. [PubMed: 22746278]

[41]. Suenaga K, Sato Y, Liu Z, Kataura H, Okazaki T, Kimoto K, Sawada H, Sasaki T, Omoto K, Tomita T, Kaneyama T, Kondo Y, Nat. Chem. 2009, 1, 415. [PubMed: 21378897]

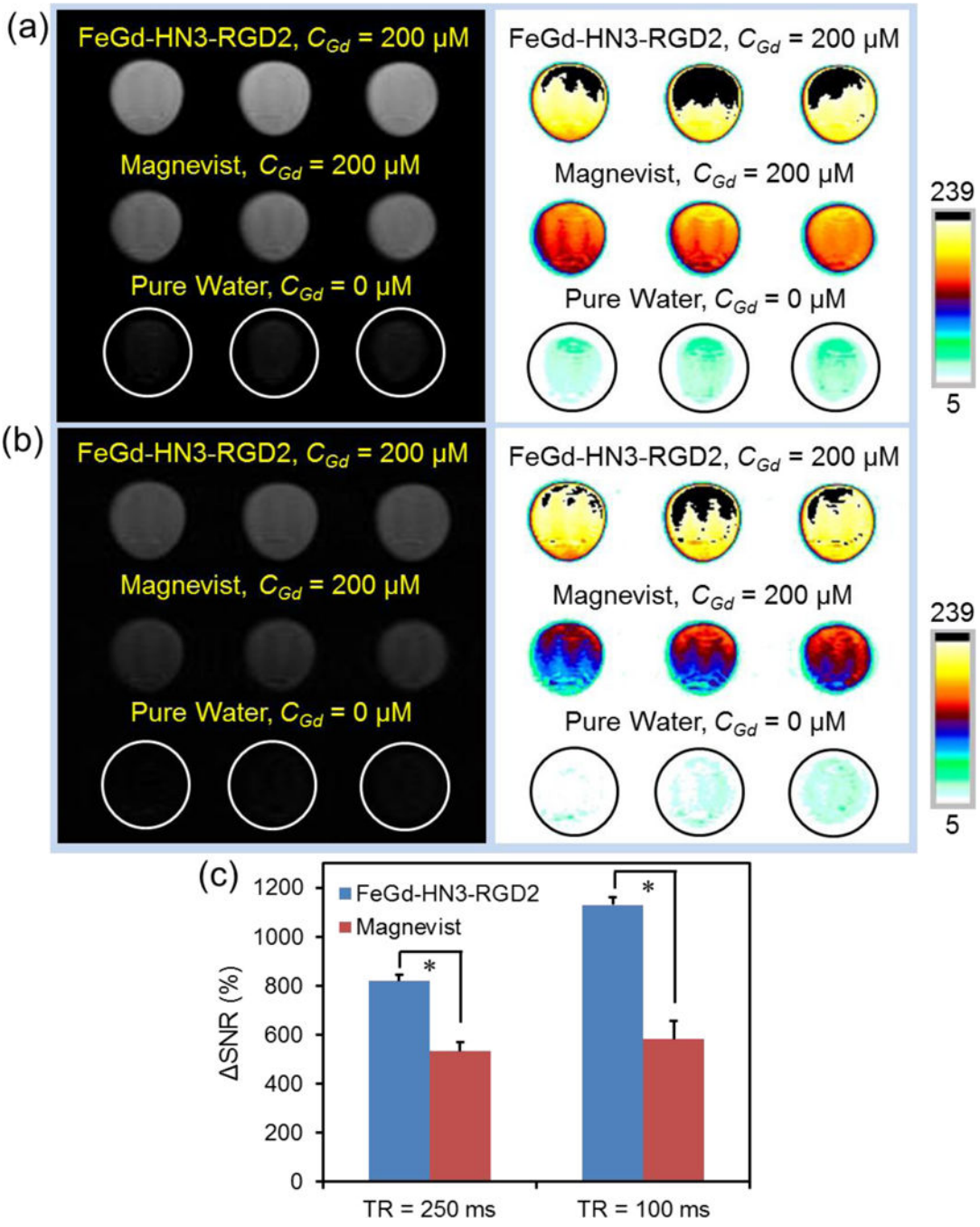

Figure 1.

T_1-weighted MR images of our FeGd-HN3-RGD2 and Magnevist® solutions (C_{Gd} = 200 μM) compared with the pure water (control) with 250 ms of TR (a), or 100 ms of TR (b). TE = 10 ms. Magnetic field = 7.0 T. (c): ΔSNR of the MR images for our FeGd-HN3-RGD2 and Magnevist® solutions compared to pure water as shown in a and b, measured by ImageJ. * P < 0.001. The SNR and ΔSNR were respectively calculated according to the equation (1) and (2).

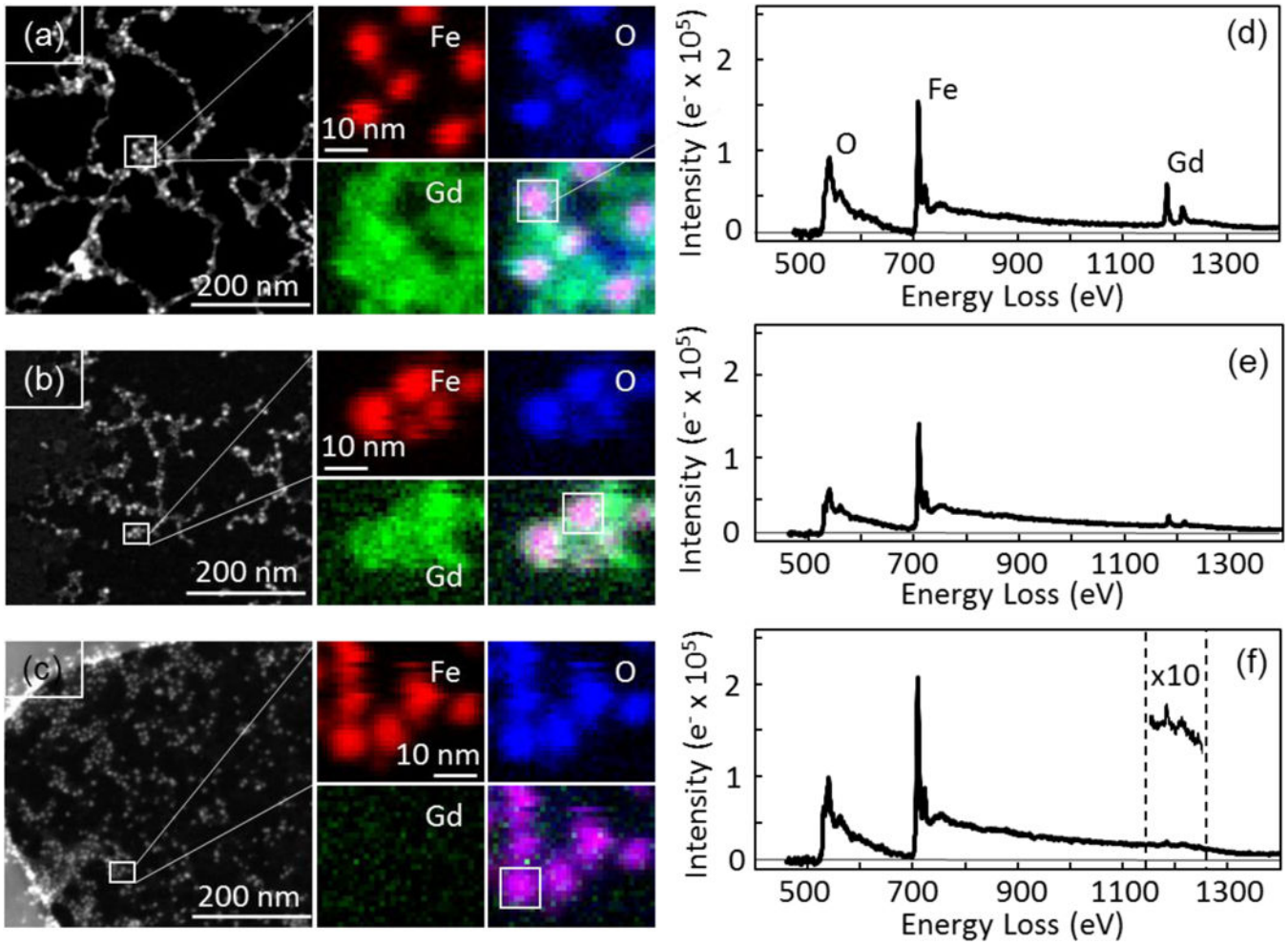

Figure 2.

Characterization of scanning transmission electron microscope (STEM), electron energy loss spectroscopic imaging (EELSI) (a-c), and EELS spectra (d-f) for the FeGd-HN1 (a, d), FeGd-HN3 (b, e), and FeGd-HN6 (c, f) nanoparticles. STEM image (left panel) is shown with small outlined region (white box), from which EELSI data were acquired. Fe (red), O (blue), and Gd (green) maps were generated for each particle by integrating 10–20 eV windows above each core edge: Fe $L_{2,3}$ edge at 710 eV, O K edge at 530 eV, and Gd $M_{4,5}$ edge at 1185 eV. Overlay images showing all three colors reveal that Gd oxide surrounds the iron oxide cores with a concentration that is greatest for FeGd-HN1 and least for FeGd-HN6. EELS spectra integrated over 10 nm × 10 nm areas containing the particle (white squares in overlay images) also show a decrease in Gd concentration from FeGd-HN1 to FeGd-HN3. For FeGd-HN6, the Gd signal is only evident after multiplying the intensity scale 10 times (inset).

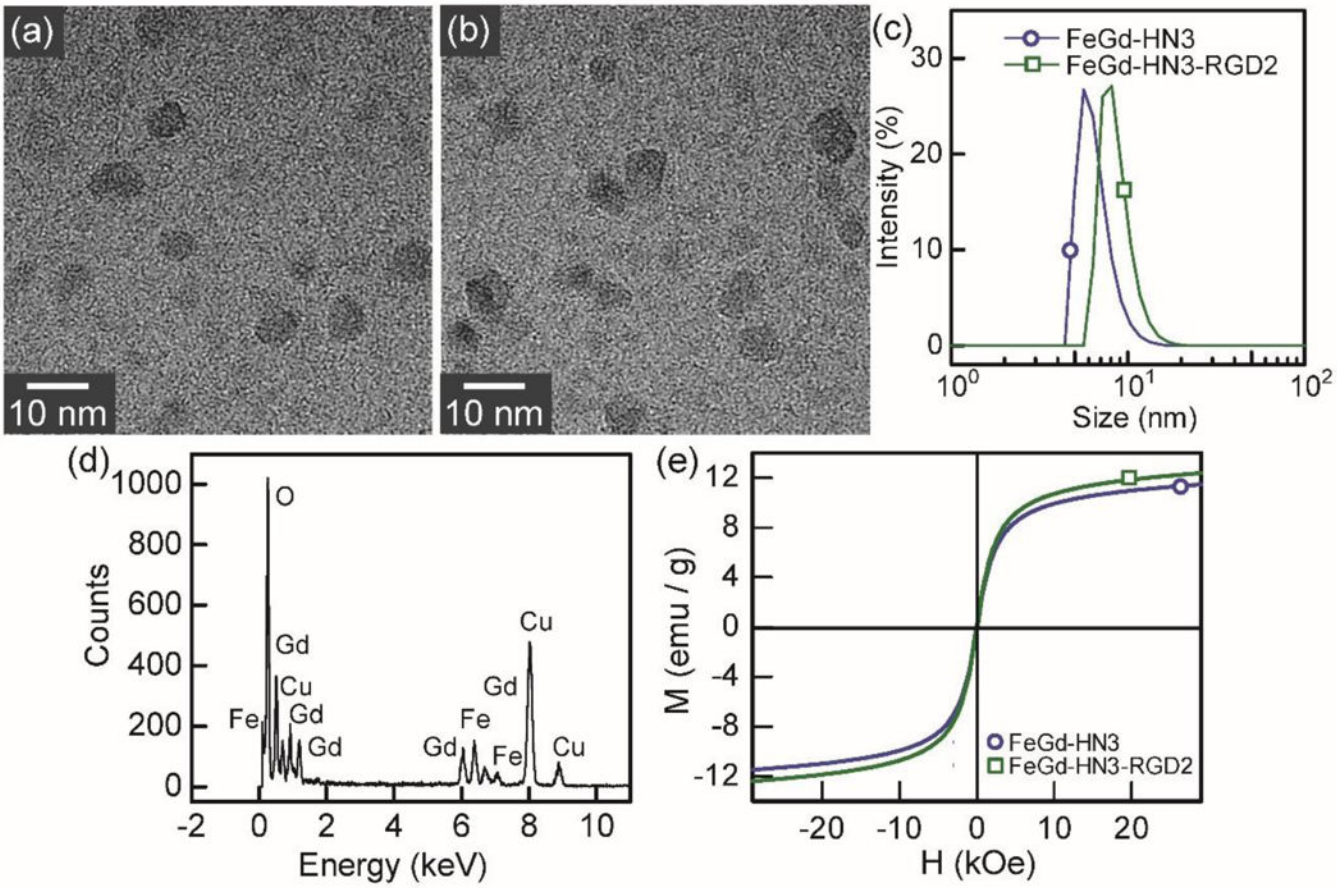

Figure 3.

Characterization of FeGd-HN3 and FeGd-HN3-RGD2. (a, b): High resolution TEM (HR-TEM) images of FeGd-HN3 (a) and FeGd-HN3-RGD2 (b). (c): Size distribution of FeGd-HN3 (d_h = 6.5 nm) and FeGd-HN3-RGD2 (d_h = 8.5 nm) measured by DLS. (d): Energy dispersive X-ray spectra (EDS) of FeGd-HN3. (e): Field-dependent magnetization curves (H-M) of FeGd-HN3 and FeGd-HN3-RGD2 at 300 K. The saturation magnetization (Ms) value was determined to be 11.5 or 12.4 emu/g for FeGd-HN3 or FeGd-HN3-RGD2.

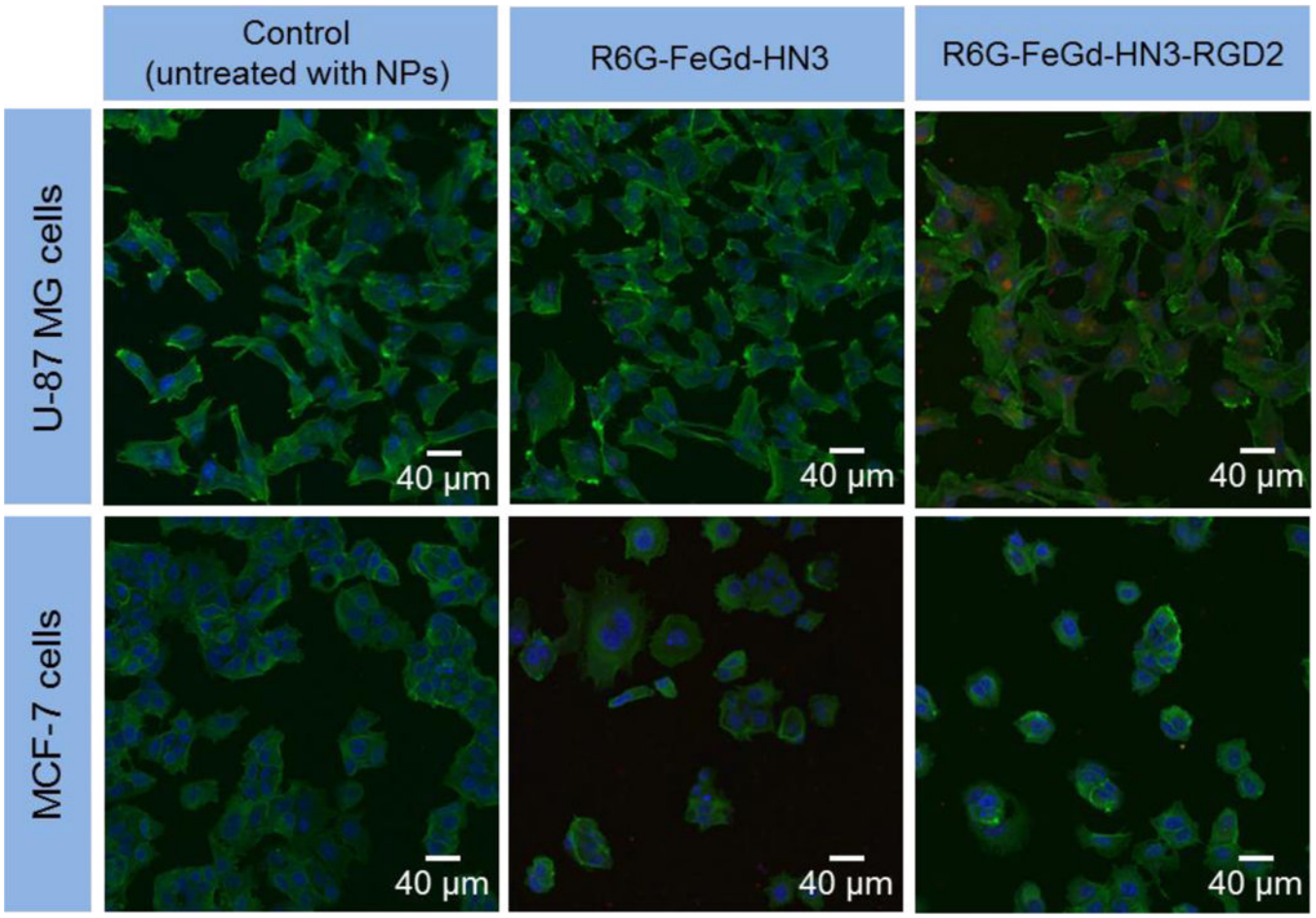

Figure 4.

LSCM images of U-87 MG or MCF-7 cells incubated with R6G-FeGd-HN3 or R6G-FeGd-HN3-RGD2. The cells untreated with nanoparticles are used as the control. The cytoskeleton stained with phalloidin-FITC is green and the nucleus stained with Hoechst is blue. The R6G-loaded nanoparticles are red.

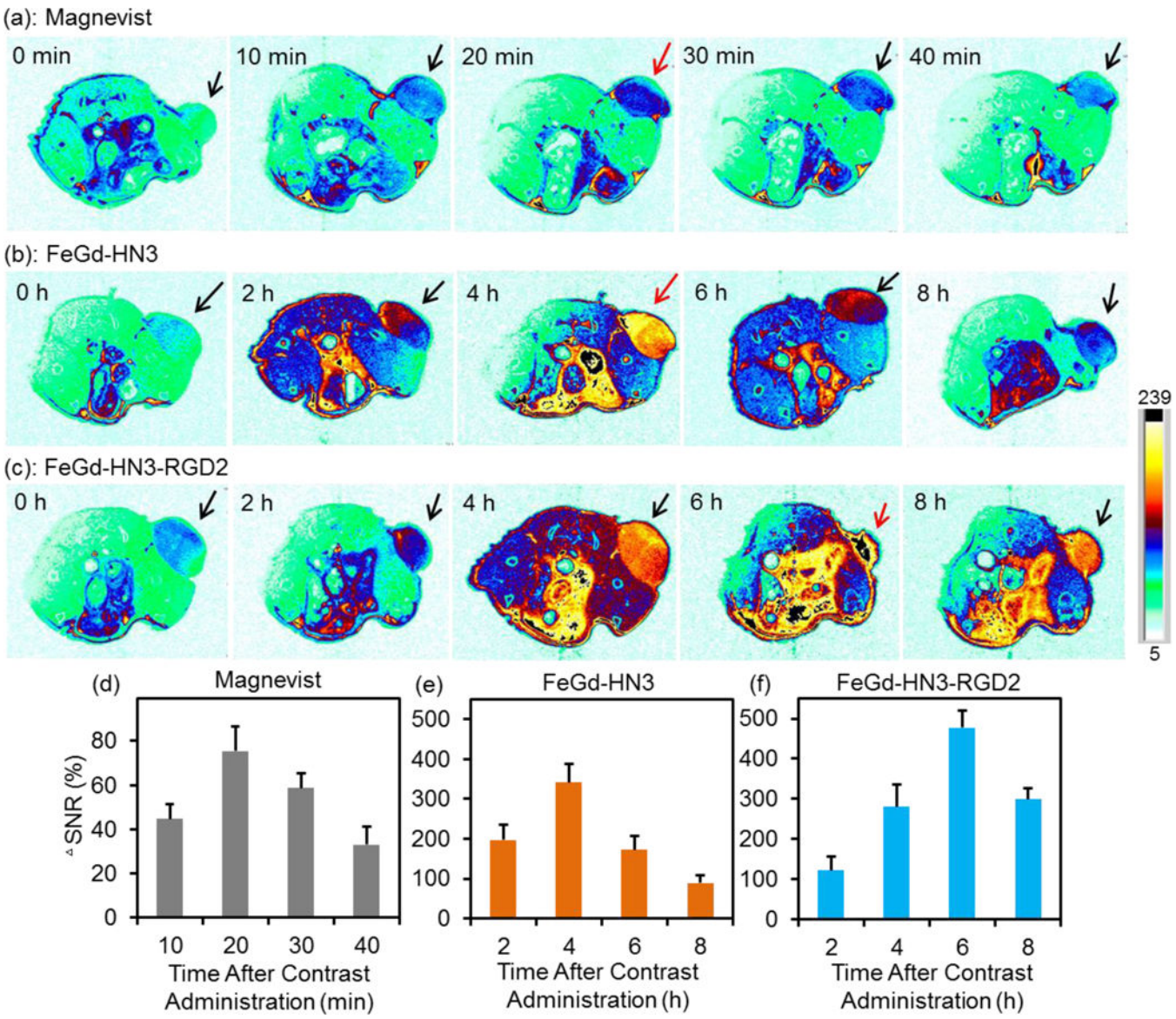

Figure 5.

In vivo T_1-weighted MR images of U-87 MG tumor-bearing nude mice (slice orientation: axial) (a-c) and quantification of the tumors (d-f) after intravenous injection of Magnevist, FeGd-HN3, or FeGd-HN3-RGD2. The Gd dosage is 5.0 mg / kg. The MR images before injection are identified as 0 h in a-c. The signal changes in tumors at different time points after contrast administration are quantified using ΔSNR. The color bar is the same for Figure 5 a, b, c.

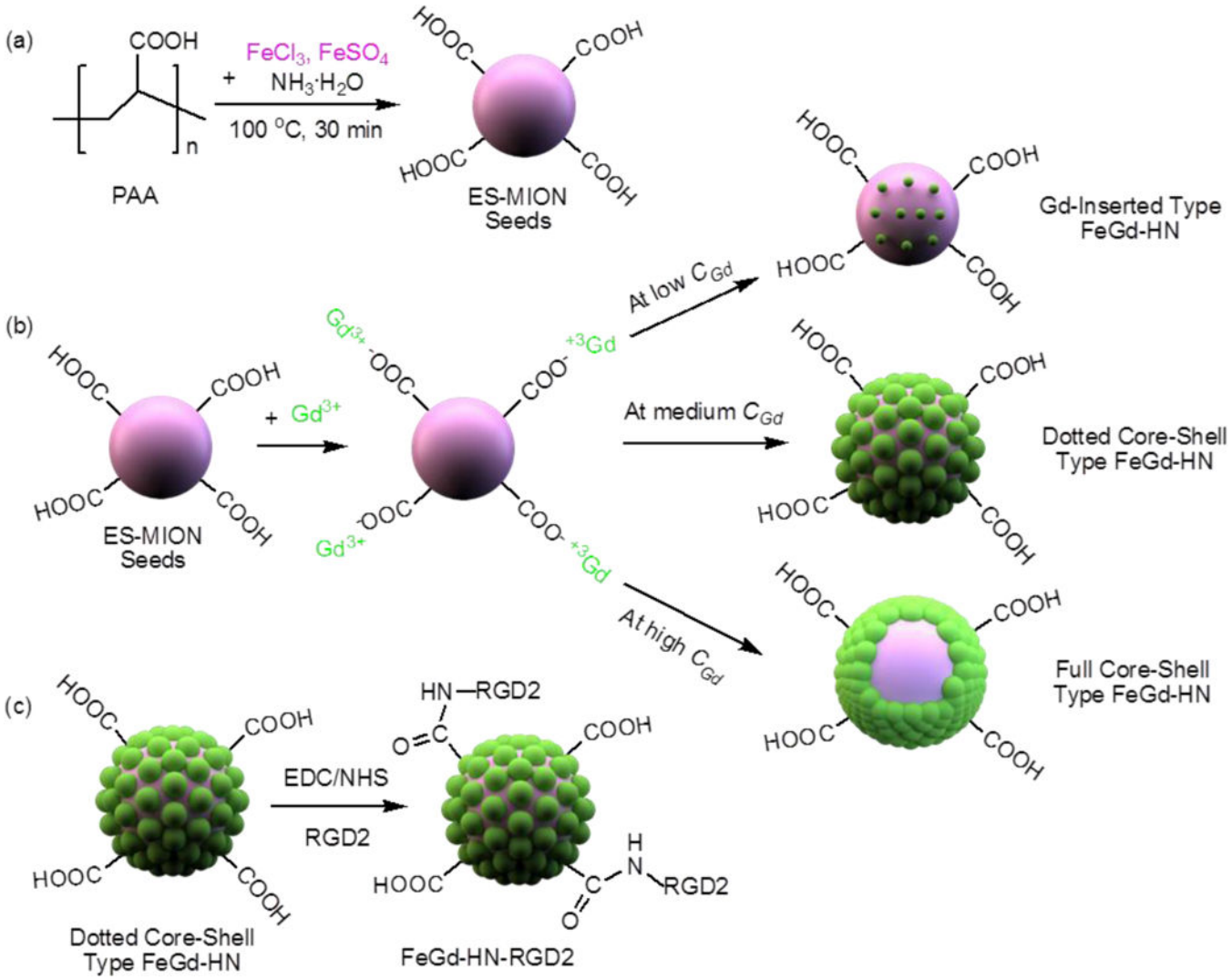

Scheme 1.

Schematic illustration of synthesis steps of our RGD2-conjugated dotted core-shell type ES-MION/GdON hybrid nanoparticles (FeGd-HN) with superhigh r_1 and very low r_2/r_1 for high contrast T_1-weighted MRI. (a): The seeds of ES-MIONs were synthesized using PAA as a stabilizer. (b): Gd^{3+} ions are adsorbed on the surfaces of ES-MION seeds via formation of ionic bonds between them and the –COOH groups from PAA, and then GdON are synthesized in situ on the surfaces of ES-MION seeds to form three different structures at different C_{Gd}. The dotted core-shell type FeGd-HN have superhigh r_1 and very low r_2/r_1, and can be used for high contrast T_1-weighted MRI. (c): The targeted ligand RGD2 is conjugated onto the surface of the dotted core-shell type FeGd-HN to construct FeGd-HN-RGD2 nanoparticles.

Table 1.

r_1 and r_2 values under different magnetic fields

Sample Nomenclature	H_0 (T) [a]	r_1 (mM^{-1} s^{-1}) (Fe+Gd) [b]	r_2 (mM^{-1} s^{-1}) (Fe+Gd) [b]	r_2/r_1 [b]	r_1 (mM^{-1} s^{-1}) (Gd) [c]	r_2 (mM^{-1} s^{-1}) (Gd) [c]	r_2/r_1 [c]
FeGd-HN3	7.0	6.92±0.42	47.4±2.2	6.86±0.31	21.0±1.3	143.9±2.9	6.86±0.31
	1.5	25.1±0.9	48.9±0.9	1.95±0.07	73.5±2.6	143.0±2.7	1.95±0.07
FeGd-HN3-RGD2	7.0	7.07	48.1	6.80	20.7	140.5	6.80
	1.5	24.0	47.6	1.98	70.0	139.2	1.98
Magnevist®	7.0	3.54	5.22	1.47	3.54	5.22	1.47
	1.5	4.25±0.07	4.51±0.02	1.06±0.02	4.25±0.07	4.51±0.02	1.06±0.02

[a] The r_1 and r_2 are measured on a MRI scanner system (7.0 T, Bruker, B-C 70/16 US), and a clinical MRI scanner system (1.5 T, Magnetom Avanto, Siemens, Germany)

[b] Calculated according to the sum of Fe and Gd concentrations (mean ± SD, $n = 3$).

[c] Calculated according to the Gd concentrations (mean ± SD, $n = 3$).